Performance Analysis of a Downlink mmWave Communication in an IRS-Based Large-scale MIMO Networks

Beyza Onal and Nihat Kabaoglu, *Member, IEEE*

***Abstract*—The tremendous advances in communication technologies require next-generation communication systems to be optimally designed in terms of speed, reliability, cost, energy consumption, spectral efficiency, ecosystem compatibility, and sustainability. With these requirements in mind, this paper discusses downlink millimeter wave communication for a large-scale multiple-input multiple-output system equipped with a group of intelligent reconfigurable surfaces, one of the potential candidates for 6G wireless networks, considering 5G physical mmWave channel models. In addition to the precoder, beamformer, and combiner design of the proposed system model, the theoretical average pairwise error probability and achievable rate expressions are derived. Furthermore, an upper bound for the achievable rate is derived. Simulation results clearly show that the performance of the proposed model is close to the theoretical bounds of the performance metrics and clearly demonstrates its superiority compared to a similar model based on index modulation.**

***Index Terms*—6G, mmWave, massive MIMO, reconfigurable intelligent surface, hybrid beamforming, index modulation.**

I. Introduction

With the rapid development of electronic devices and computer technologies, many applications in our lives have provided a great increase in wireless data traffic in recent years. Next-generation mobile networks are therefore expected to meet demands such as high data rate, high spectral efficiency (SE), low latency, etc. [1], [2]. Since existing spectrum resources cannot meet increasing user demands, communication systems using higher frequency bands, called millimeter wave (mmWave) communication have been proposed [3], [4].

mmWave communication is a promising alternative technology using its advantages such as wide spectrum area of 30–300 GHz, high SE, and high data rate, but it has a serious propagation path loss problem [4], [5], [6], [7]. In addition, the small wavelengths of the mmWave frequency bands allow more antenna elements to be placed per unit physical area [8]. This makes it possible to design large-scale multiple-input multiple-output (Ls-MIMO) systems. The application of Ls-MIMO systems at mmWave frequencies has slightly solved the highlighted path loss problem by providing high antenna gain [3], [5], [9]. However, the mmWave Ls-MIMO systems need a large number of radio frequency (RF) chains, and that results in high power consumption and hardware cost [5], [6], [7], [8]. The hybrid beamforming (HB) technique has thus become an inherent part of the mmWave Ls-MIMO systems as it greatly reduces hardware cost and power consumption [4], [7], [10], minimizes inter-signal interference and also provides high SE [11], [12], but there is a serious performance degradation compared to the fully digital one. To compensate for the performance loss and to reduce the hardware cost further, index modulation (IM) based studies in [13] and [14] are proposed.

The authors in [13] propose spectral path IM to increase multiplexing gain and a federated learning-based beamformer design. Their proposed method exhibits lower SE performance than the model-based one. Moreover, this performance degrades as the gain difference among the propagation paths increases. Also, its bit error rate (BER) performance is ambiguous since it is not addressed. In [14], a system in which spatial modulation (SM) is applied to the HB of multi-user (MU) mmWave networks is proposed and shown to provide higher SE and BER performance compared to the classical SM technique. However, since the theoretical BER curve is not presented as a lower bound in this study, the actual performance of this method cannot be fully understood. Despite the highlighted advantages, the performance loss of the system model proposed in [14] remains a great real practical problem, since the high path loss at mmWave frequencies isn't taken into account.

Intelligent reconfigurable surface (IRS) technology has been a promising solution to improve that performance loss as well as increase the SE of wireless networks with low-cost hardware structure and with minimum energy consumption [12], [15], [16], [17], [18]. Most of the recent works have focused on the joint design of the IRS reflection matrix and hybrid beamformer, and have considered point-to-point communication for a model with a single IRS [17], [18], [19], [20], [21]. In [22], the authors proposed a cost-effective and efficient new algorithm framework for channel capacity maximization through common antenna selection, and passive beamforming in IRS-assisted Ls-MIMO systems. In [23], an IRS-assisted and angular-based hybrid beamforming technique is proposed for mmWave Ls-MIMO

Manuscript received 28 December 2023; revised 17 April 2024 and 25 June 2024; accepted 6 August 2024. Date of publication 14 August 2024; date of current version 19 December 2024. The review of this article was coordinated by Prof. Yue Gao. *(Corresponding author: Nihat Kabaoglu.)*

The authors are with the Department of Electrical and Electronic Engineering, Istanbul Medeniyet University, 34857 Istanbul, Türkiye (e-mail: beyza.onal@medeniyet.edu.tr; nihat.kabaoglu@medeniyet.edu.tr).

Digital Object Identifier 10.1109/TVT.2024.3443098

systems, and it is shown with numerical results that a remarkable increase in achievable rate performance is achieved by effectively positioning of IRS. In [24], an IRS-assisted beam selection algorithm with maximum-minimum fairness power allocation is proposed, and it is proven to outperform conventional schemes.

Keeping the advantages of the model in [14], we think that its BER performance and SE can be improved further using a group of IRS under even a realistic channel model for mmWave frequencies. With this motivation, in this study, a new system model in which a multi-IRS scheme is integrated into the HB configuration of multi-user Ls-MIMO systems for downlink mmWave communication is introduced, analog beamformer, digital combiner, and digital precoder are designed, theoretical BER and theoretical SE are derived, and thus a complete downlink system analysis is presented under a realistic channel model.

In our proposed system, multiple IRSs are placed among the base station (BS) and the mobile stations (MSs) to assist direct communication. Since a mmWave cellular network inherently consists of small cells, locating all IRSs close to each other in a cell is inevitable. Therefore, which IRS is active during communication does not have a significant impact on system performance in this type of cell. Hence, there is no need for an algorithm that determines which IRS is active in this work. The data bits from the source use the SM technique to determine which RISs are active during communication, thus achieving a higher SE. Since IRSs can be deployed densely and quickly without introducing additional interference, while achieving controllable costs and low power consumption, no significant additional installation cost or complexity arises in the control and feedback channels [25]. Through IRSs, the reflected signal is aligned to the phase of the signal arriving at the receiver directly, thus increasing the signal strength at the receiver. To maximize SE, data symbols, uniform linear arrays' (ULAs) indices, and IRSs' indices information are carried together in a frame. These indices are determined using the SM technique by using the incident data bit streams on the BS side. The selected IRS information is relayed from the BS to the IRS controller, which activates one. Ultimately, since only one of the multiple antenna arrays and one of the multiple IRSs are active for only one user, the need of synchronization among antennas and IRSs is removed and interference is widely avoided. Thus, high BER performance, high data rate, and high SE are achieved as a whole.

A. Contributions

The main contribution of this paper to the literature is to show that a small cell-based system model with multiple IRSs using mmWave frequencies (28 GHz and 73 GHz) can also improve BER performance and further increase spectral efficiency. To achieve this main objective, the following contributions have been made:

- In order to maximise SE (and hence data rate) and improve BER performance while eliminating Inter-User Interference (IUI) and minimising system cost, we propose a novel system model based on IRS selection, where multiple IRSs are placed between BSs and MSs in the form of HB-structured mmWave Ls-MIMO systems with SM scheme.
- According to the proposed system model, an analog beamformer, a digital combiner and a digital precoder are designed. The computational complexity of the designed analog beamformer, digital precoder, and combiner is calculated and compared with the computational complexity of other widely used methods in downlink systems.
- We derive both the theoretical achievable rate and its upper bound, as well as the theoretical BER of our proposed system using pairwise error probability (PEP), and compare them to the study using the SM scheme in [14].
- We analyze the performance of the proposed system model in two subsections: Classical Channel Model and Real Physical Channel Model. We use the 5G UMi-Street Canyon and 5G InH Indoor-Office path loss models at 28 GHz and 73 GHz to experience a real physical radio channel in indoor and outdoor environments.

B. Organization and Notation

The rest of the article is organized into the following sections. In Section II, the proposed system model is introduced and the design of the analog beamformer, digital precoder, digital combiner, and receiver structure are presented. Section III represents the theoretical BER analysis and Section IV represents the achievable rate analysis. In Section V, simulation results are presented and discussed. Finally, the conclusion of the article is given in Section VI.

Throughout the paper, scalar values are italicized, and vectors/matrices are presented by bold lower/upper case symbols. $(.)^T$, $(.)^H$, E$\{.\}$, $tr(.)$, $|.|$, $||.||$, and $(.)^\dagger$ denote the transpose, the conjugate transpose, the expectation operatör, the trace of the matrix, the absolute value, the ℓ_2 norm, and the pseudo-operation, respectively. $\Re e$ and $\Im m$ represent the real and imaginary components of the complex value. $\mathcal{CN}(0, \sigma^2)$ represents the circular symmetric complex Gaussian distribution with zero mean and variance σ^2.

II. System Model

Our proposed system model, Multi-IRS-HB, is discussed for two subsections, Classical Channel Model and Real Physical Channel Model. The proposed MU Ls-MIMO system consists of one BS with N_U ULAs serving C number of users with N_R receive antennas. Each of ULAs has N_T transmit antennas. It is assumed that X number of IRSs, each consisting of N_S reflective elements, are placed in the optimal location between BS and MSs in a small cell (i.e., the building roof or facade for outdoor scenarios and the ceiling or an interior wall near the ceiling for indoor scenarios) and the communication protocol is time division duplex. It is shown in Fig. 1. In the system, according to the use of the SM, the bit stream to be transmitted to a target user consists of three parts, $\log_2 N_U$, $\log_2 X$ and $\log_2 M$. The first and second part indicate which ULA and IRS are selected for transmission while the last part indicates a symbol from M-ary symbol alphabet. For each bit stream, one of the ULAs and one of the IRSs are selected depending on the incoming bits, and

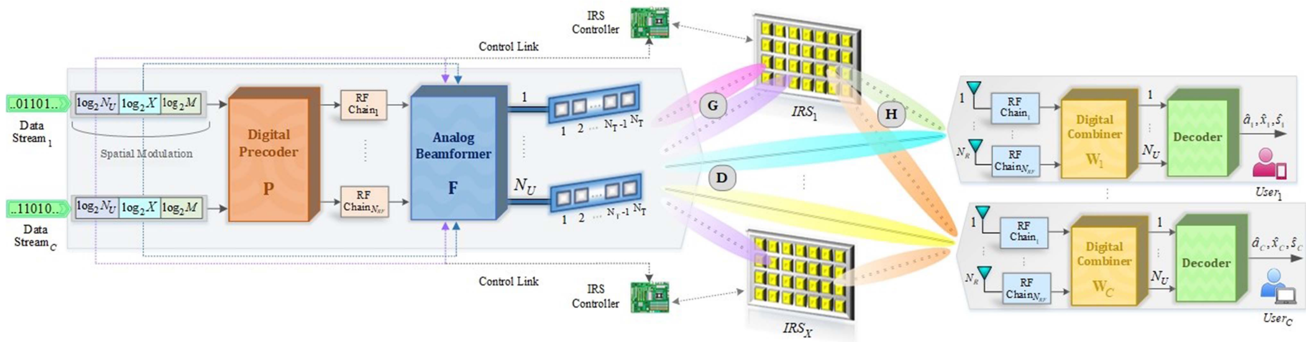

Fig. 1. System model of multi-user Ls-MIMO with multi-IRS assisted for downlink mmWave communication.

M-ary modulated data is transmitted using the selected ULA and IRS. Thus, the active ULA and IRS indices carry information together without consuming additional power. In the considered system, downlink communication is established in two different ways: i) Direct transmission from a_v-th ULA to k-th user, ii) Transmission from a_v-th ULA with the help of i_x-th IRS to k-th user, where $a_v \in \{1,\ldots,N_U\}, i_x \in \{1,\ldots X\}$ and $k \in \{1,\ldots,C\}$ represent the ULA index, IRS index, and intended user index, respectively. The total number of bits conveyed by only one data stream is $b_t = \log_2 N_U + \log_2 X + \log_2 M$.

A. Classical Channel Model

After the C bit streams arrive in the transmission chains of the BS, indices of ULA and IRS are obtained for each user using the SM bits. Then, the BS generates the digital precoder and determines the analog beamformer, both of which are explained in the next section. The signal at k-th user can be written as:

$$\mathbf{r}_k = \sqrt{P}\sum_{v=1}^{C}\mathbf{Y}_{a_v,i_v,k}\mathbf{f}_{a_v,i_v,v}\mathbf{p}_{a_v,i_v,v}\mathbf{s}+\mathbf{n}_k, \tag{1}$$

where $\mathbf{Y}_{a_v,i_v,k} = \mathbf{D}_{a_v,k} + \mathbf{H}_{i_v,k}\boldsymbol{\Theta}_{i_v}\mathbf{G}_{a_v,i_v}$ is the total combined channel from source to destination. Therein, $\mathbf{D}_{a_v,k} \in \mathbb{C}^{N_R\times N_T}$, $\mathbf{G}_{a_v,i_v} \in \mathbb{C}^{N_S\times N_T}$, and $\mathbf{H}_{i_v,k} \in \mathbb{C}^{N_R\times N_S}$ denote direct channel from i_v-th ULA of the BS to k-th MS, channel from the BS to i_v-th IRS, and channel from i_v-th IRS to k-th MS, respectively. $\boldsymbol{\Theta}_{i_v} = \mathrm{diag}([e^{j\theta_1},\ldots,e^{j\theta_{N_S}}]) \in \mathbb{C}^{N_S\times N_S}$ is reflection matrix of the IRSs and $\theta_{n_S} \in [0,2\pi)$ describes phase shift of n_s-th IRS element, $n_s \in \{1,\ldots,N_S\}$. The reflection phases of the reflecting surfaces are provided by the IRS controller via the control link from the BS to the IRS, as seen in Fig. 1. P represents the total transmit power and it is assumed that each user is allocated equal power since equal power allocation in large-scale MIMO systems where the number of BS antennas is larger than the number of receive antennas $N_T \gg N_R$ results in a negligible performance degradation compared to the optimized solution [26]. $\mathbf{s} \in \mathbb{C}^{C\times 1}$ is symbol vector consisting of M-ary modulated signals, and $\mathbf{n}_k \in \mathbb{C}^{N_R\times 1} \sim \mathcal{CN}(0,\sigma^2)$ is the circularly symmetric complex Gaussian noise vector where the elements follow an identically distributed (i.i.d.) distribution. $\mathbf{p}_{a_v,i_v,v} \in \mathbb{C}^{1\times C}$ and $\mathbf{f}_{a_v,i_v,v} \in \mathbb{C}^{N_T\times 1}$ are the digital precoding and analog beamforming vectors for transmission from a_v-th ULA with the help of i_v-th IRS to k-th user, respectively. The channels[1] are modeled as follows:

$$\mathbf{D}_{a_v,k} = \sqrt{\frac{N_T N_R}{L_D}}\sum_{l_d}^{L_D}\alpha_{a_v,k}^{l_d}\mathbf{a}_{R_{a_v,k}}(\chi_{l_d})\mathbf{a}_{T_{a_v,k}}^H(\upsilon_{l_d}), \tag{2}$$

$$\mathbf{G}_{a_v,i_v} = \sqrt{\frac{N_T N_S}{L_G}}\sum_{l_g}^{L_G}\alpha_{a_v,i_v}^{l_g}\mathbf{a}_{R_{i_v,a_v}}(\lambda_{l_g})\mathbf{a}_{T_{a_v,i_v}}^H(\beta_{l_g}), \tag{3}$$

$$\mathbf{H}_{i_v,k} = \sqrt{\frac{N_S N_R}{L_H}}\sum_{l_h}^{L_H}\alpha_{i_v,k}^{l_h}\mathbf{a}_{R_{a_v,k}}(\delta_{l_h})\mathbf{a}_{T_{i_v,k}}^H(\gamma_{l_h}). \tag{4}$$

As can be seen from the equations, the system has a multipath fading channel model, $l_d = \{1,\ldots,L_D\}, l_g = \{1,\ldots,L_G\}, l_h = \{1,\ldots,L_H\}$. L_D, L_G, and L_H are the numbers of the paths of the BS-MS, the BS-IRS, and the IRS-MS channels, respectively. $\alpha_{a_v,k}^{l_d}, \alpha_{a_v,i_v}^{l_g}$, and $\alpha_{i_v,k}^{l_h}$ are the path gains following the circular symmetric complex Gaussian distribution, $\mathcal{CN}(0,1)$. υ_{l_d}, β_{l_g}, γ_{l_h} are the angle of departure and χ_{l_d}, λ_{l_g}, δ_{l_h} are the angle of arrival of the respective path and all are uniformly distributed, $U(0,2\pi]$. $\mathbf{a}_{R_{a_v,k}}(\chi_{l_d})$ and $\mathbf{a}_{T_{a_v,k}}(\upsilon_{l_d})$, $\mathbf{a}_{R_{i_v,a_v}}(\lambda_{l_g})$ and $\mathbf{a}_{T_{a_v,i_v}}(\beta_{l_g})$, $\mathbf{a}_{R_{a_v,k}}(\delta_{l_h})$ and $\mathbf{a}_{T_{i_v,k}}(\gamma_{l_h})$ denote the receiver and transmitter antenna array responses of l_d-th, l_g-th, and l_h-th path respectively and the antenna array response for N antennas is formulated as follows:

$$\mathbf{a}(\phi_l) = \sqrt{\frac{1}{N}}[1, e^{j\pi\sin\phi_l},\ldots,e^{j\pi(N-1)\sin\phi_l}]^T, \tag{5}$$

where the arrays in which elements of the ULA and IRS are separated by half a wavelength are considered, that is, $d_{ULA} = \lambda/2$.

B. Real Physical Channel Model

In this section, the proposed system model is discussed under different path loss models. The channel equations given in (2), (3), and (4) can be rewritten as follows, considering the path loss coefficients:

$$\mathbf{D}_{a_v,k} = \sqrt{\frac{N_T N_R}{PL_{k_{l_d}}^{BG}L_D}}\sum_{l_d}^{L_D}\alpha_{a_v,k}^{l_d}\mathbf{a}_{R_{a_v,k}}(\chi_{l_d})\mathbf{a}_{T_{a_v,k}}^H(\upsilon_{l_d}), \tag{6}$$

[1]They are also known as Saleh-Valenzuela channel models.

$$\mathbf{G}_{a_v,i_v} = \sqrt{\frac{N_T N_S}{PL^{BY}_{k_{l_g}} L_G}} \sum_{l_g}^{L_G} \alpha^{l_g}_{a_v,i_v} \mathbf{a}_{R_{a_v,i_v}}(\lambda_{l_g}) \mathbf{a}^H_{T_{a_v,i_v}}(\beta_{l_g}), \tag{7}$$

$$\mathbf{H}_{i_v,k} = \sqrt{\frac{N_S N_R}{PL^{YG}_{k_{l_h}} L_H}} \sum_{l_h}^{L_H} \alpha^{l_h}_{i_v,k} \mathbf{a}_{R_{i_v,k}}(\delta_{l_h}) \mathbf{a}^H_{T_{i_v,k}}(\gamma_{l_h}). \tag{8}$$

Therein, the parameters $PL^{BG}_{k_{l_d}}$, $PL^{BY}_{k_{l_g}}$, and $PL^{YG}_{k_{l_h}}$ represent the path loss coefficient of the corresponding path. Path loss on a link can also be represented in vector form as $\mathbf{PL}^{BG}_k = [PL^{BG}_{k_{l_{d_1}}}, \ldots, PL^{BG}_{k_{l_D}}]$, $\mathbf{PL}^{BY}_k = [PL^{BY}_{k_{l_{g_1}}}, \ldots, PL^{BY}_{k_{l_G}}]$, and $\mathbf{PL}^{YG}_k = [PL^{YG}_{k_{l_{h_1}}}, \ldots, PL^{YG}_{k_{l_H}}]$. Path losses in the system are generated by considering 5G UMi-Street Canyon for the outdoor environment and 5G InH Indoor-Office model for the indoor environment.

1) Path Loss Model for Indoor Environment: 5G InH Indoor-Office models are respectively expressed for line-of-sight (LOS) and non-LOS (NLOS) transmission as follows [28]:

$$PL_{LOS} = 17.3\log_{10}(d) + 32.4 + 20\log_{10}(f_c), \tag{9}$$

$$PL_{NLOS} = 38.3\log_{10}(d) + 17.30 + 24.9\log_{10}(f_c), \tag{10}$$

where f_c represents the carrier frequency in GHz and d represents the distance between stations in m.

2) Path Loss Model for Outdoor Environment: 5G UMi-Street Canyon models are respectively expressed for LOS and NLOS transmission as follows [28]:

$$PL_{LOS} = 21\log_{10}(d) + 32.4 + 20\log_{10}(f_c), \tag{11}$$

$$PL_{NLOS} = 31.7\log_{10}(d) + 32.4 + 20\log_{10}(f_c). \tag{12}$$

Using the above equations, path loss coefficient pairs of the proposed system are formed as $PL^{SD}_{k_{LOS}}$ and $PL^{SD}_{k_{NLOS}}$, $PL^{SR}_{k_{LOS}}$ and $PL^{SR}_{k_{NLOS}}$, $PL^{RD}_{k_{LOS}}$ and $PL^{RD}_{k_{NLOS}}$ which represent the path loss coefficient pairs of BS-MS, BS-IRS, and IRS-MS links, respectively. $d_{k_{l_d}}$, $d_{k_{l_g}}$, and $d_{k_{l_h}}$ are link distances, and link distance vectors are expressed as $\mathbf{d}^{SD}_k = [d_{k_{l_{d_1}}}, \ldots, d_{d_{k_{L_D}}}]$, $\mathbf{d}^{SR}_k = [d_{k_{l_{g_1}}}, \ldots, d_{k_{d_{L_G}}}]$ and $\mathbf{d}^{RD}_k = [d_{k_{l_{h_1}}}, \ldots, d_{k_{d_{L_H}}}]$.

C. Analog Beamformer, Digital Combiner, and Digital Precoder Design

In order to combat the poor scattering nature of mmWave channels, BS uses analog beamformers to get a high beamforming gain. Codebook-based beamforming methods offer less complexity and satisfactory performance due to the special structure of the hybrid beamformer and the characteristics of mmWave MIMO channels. Therefore, we prefer the codebook-based beamforming design in our system model.

First, a set of codewords S_{F_T} is constituted. Each vector element of this set, $\mathbf{f}_t \in \mathbb{C}^{N_T \times 1}$, consists of analog beamforming vectors generated for each of $T = 2^R$ different angles in the range $(0, 2\pi]$, i.e., the codebook for the quantized angle $\theta_t = \frac{2\pi t}{T}$ for $t \in \{0, 1, \ldots, T-1\}$ is

$$\mathbf{f}_t = \sqrt{\frac{1}{N_T}} \left[1, e^{j\pi \sin(\theta_t)}, \ldots, e^{j\pi(N_T-1)\sin(\theta_t)}\right]^T.$$

The optimal analog beamforming vector $\mathbf{f}_t$ which maximizes the signal-to-noise ratio (SNR) of the channel $\mathbf{Y}_{a_v,i_x,k}$ is searched by independently solving the following optimization problem for each ULA–IRS-user triplet

$$\mathbf{f}_{a_v,i_x,k} = \underset{\forall \mathbf{f}_t \in S_{F_T}}{\arg\max} \|\mathbf{Y}_{a_v,i_x,k}\mathbf{f}_t\|^2. \tag{13}$$

Therefore, the search space of the optimization problem is S_{F_T} with cardinality $\mathbf{card}(S_{F_T}) = T$ which generally is not a large number. Hence, the brute-force method is adopted to provide the optimum solution since the problem size is limited. The optimum analog beamformers for each ULA–IRS-user triplet are obtained at the beginning of each coherence time of the channel and are stored at the BS. Computational complexity of this method for each ULA–IRS-user triplet is $\mathcal{O}(TN_RN_T)$. According to the ULA and IRS selected based on the incoming bitstream, the final analog beamforming matrix for all users is as $\mathbf{F} = [\mathbf{f}_{a_1,i_1,1}, \ldots, \mathbf{f}_{a_C,i_C,C}] \in \mathbb{C}^{N_T \times C}$.

In the downlink, the most common linear precoding and combining schemes are matched filter (MF) (also known as maximum ratio), zero forcing (ZF) and minimum mean square error (MMSE). Although the MF scheme has the worst performance among these three methods, it has the lowest computational complexity and it is possible to obtain its closed-form expression easily. The MMSE scheme has the highest performance among them. However, it is quite difficult to find a closed-form solution for this method. In addition, the capacity expression is quite complex. The ZF scheme, whose computational complexity is close to that of MMSE, has a slightly lower performance in general, but its performance approaches that of MMSE for high numbers of antennas. In addition, the closed-form expression of this scheme is easy to obtain and it eliminates inter-user interference. Because of these advantages, the ZF method is preferred for the design of the digital precoder and the digital combiner.

First, the BS generates the matrix $\mathbf{Y}_k = [\mathbf{Y}_{1,1,k}\mathbf{f}_{1,1,k}, \mathbf{Y}_{2,2,k}\mathbf{f}_{2,2,k}, \ldots, \mathbf{Y}_{N_U,X,k}\mathbf{f}_{N_U X,k}]$ for each user to be able to obtain the digital combiner. Then, the digital combiner $\mathbf{W}_k = [\mathbf{w}_{1,1,k} \ldots \mathbf{w}_{N_U,X,k}] = (\mathbf{Y}^\dagger_k)^H$ of the k-th user is calculated using $\mathbf{Y}_k$ to successfully acquire the transmitted symbol. Computational complexity of the the digital combiner is $\mathcal{O}(N_UN_RN_T) + 2\mathcal{O}(N_UN_R^2) + \mathcal{O}(N_R^3)$ for each user.

Later, BS calculates the effective channel matrix $\mathbf{Y}_{eff}$ according to the (14) shown at the bottom of the next page, to form the digital precoder to overcome the inter-user-interference. Finaly, the precoding matrix for all users is obtained as $\mathbf{P} = [\mathbf{p}^T_{a_1,i_1,1} \ldots \mathbf{p}^T_{a_C,i_C,1}]^T = \varepsilon\mathbf{Y}^\dagger_{eff}$, where $\mathbf{p}_{a_k,i_k,k} \in \mathbb{C}^{1\times C}$ represents the precoding vector of the k-th user in case the a_k-th ULA and the i_k-th IRS are selected based on the SM bits. The coefficient ε meets the average power constraint and can be calculated as $\varepsilon = \epsilon\left\{\sqrt{\frac{C}{tr(\mathbf{Y}^\dagger_{eff}(\mathbf{Y}^\dagger_{eff})^H)}}\right\}$. Computational complexity of the digital ZF precoder for all users is $\mathcal{O}(N_RN_T^2C^2) + 3\mathcal{O}(C^3)$.

Accordingly, the overall computational complexity can be found as $C \times \mathcal{O}(TN_RN_T) + \mathcal{O}(N_RN_T^2C^2) + 3\mathcal{O}(C^3) + C \times [\mathcal{O}(N_UN_RN_T) + 2\mathcal{O}(N_UN_R^2) + \mathcal{O}(N_R^3)]$. Table I is presented

TABLE I
COMPUTATIONAL COMPLEXITY

Method	Precoder	Combiner
ZF	$\mathcal{O}(N_R N_T^2 C^2) + 3\mathcal{O}(C^3)$	$C \times [\mathcal{O}(N_U N_R N_T) + 2\mathcal{O}(N_U N_R^2) + \mathcal{O}(N_R^3)]$
MMSE	$\mathcal{O}(N_R N_T^2 C^2) + 3\mathcal{O}(C^3)$	$C \times [\mathcal{O}(N_U N_R N_T) + 2\mathcal{O}(N_U N_R^2) + \mathcal{O}(N_R^3)]$
MF	$\mathcal{O}(N_R N_T^2 C^2) + \mathcal{O}(C^2)$	$C \times [\mathcal{O}(N_U N_R N_T) + \mathcal{O}(N_U N_R^2)]$

for comparison with other methods in terms of computational complexity.

D. Receiver Structure

After the combining process, the received signal at k-th user can be given as

$$y_k = \mathbf{w}_{a_k,i_k,k}^H \sqrt{P} \sum_{v=1}^{C} \mathbf{Y}_{a_v,i_v,k} \mathbf{f}_{a_v,i_v,v} \mathbf{p}_{a_v,i_v,v} \mathbf{s} + \mathbf{w}_{a_k,i_k,k}^H \mathbf{n}_k. \tag{15}$$

Since interference from other users is blocked by means of the precoder at the transmitter, the resulting signal for the k-th user is obtained as

$$y_k = \sqrt{P_k} \mathbf{w}_{a_k,i_k,k}^H \mathbf{Y}_{a_k,i_k,k} \mathbf{f}_{a_k,i_k,k} s_k + \mathbf{w}_{a_k,i_k,k}^H \mathbf{n}_k. \tag{16}$$

The MS does not know which ULA and IRS have been selected at the BS to transmit the signal to it. The decoder must therefore be designed accordingly. A maximum likelihood (ML) detector is designed to detect the indices of ULA and IRS, and transmitted symbol together, as follows

$$[\hat{a}_k, \hat{i}_k, \hat{s}_k] = \underset{\substack{a \in \{1,\ldots,N_U\} \\ i \in \{1,\ldots,X\} \\ m \in \{1,\ldots,M\}}}{\arg\min} \left\| \frac{1}{\varepsilon} \mathbf{w}_{a,i,k}^H \mathbf{r}_k - s_m \right\|^2, \tag{17}$$

where $\mathbf{w}_{a,i,k} \in \mathbb{C}^{N_R \times 1}$ is the digital combiner for the transmission from a-th ULA with the help of i-th IRS to k-th user. s_m is the m-th symbol in the M-ary alphabet. $\hat{a}_k, \hat{i}_k, \hat{s}_m$ are the estimated indices of ULA and IRS, and estimated symbol from the M-ary alphabet, respectively. Computational complexity of the ML detector is $\mathcal{O}(2CN_U N_R M)$. It is quite low even for battery-powered portable devices.

III. BIT ERROR RATE ANALYSIS

In this section, the BER performance of the proposed system is obtained by using average PEP[2] and theoretical SE are derived, and thus a complete downlink system analysis is presented under a realistic channel model. a_k, i_k and s_k represent the correct ULA, IRS and symbol, while $\hat{a}_k$, $\hat{i}_k$ and $\hat{s}_k$ represent detected ones. The average PEP of the proposed system for the received signal at k-th user y_k in (16) can be obtained as follows:

$$\begin{aligned} &P\left(\{a_k, i_k, s_k\} \rightarrow \left\{\hat{a}_k, \hat{i}_k, \hat{s}_k\right\} | \{a_k, i_k, s_k\}\right) \\ &= P\left(\left| y_k - \sqrt{P_k} \mathbf{w}_{a_k,i_k,k}^H \mathbf{Y}_{a_k,i_k,k} \mathbf{f}_{a_k,i_k,k} s_k \right|^2 \right. \\ &\left. > \left| y_{\hat{k}} - \sqrt{P_k} \mathbf{w}_{\hat{a}_k,\hat{i}_k,\hat{k}}^H \mathbf{Y}_{\hat{a}_k,\hat{i}_k,\hat{k}} \mathbf{f}_{\hat{a}_k,\hat{i}_k,\hat{k}} \hat{s}_k \right|^2 \right). \end{aligned} \tag{18}$$

The average PEP analysis of the proposed system should be considered for four different cases: i) ULA and IRS are detected correctly: $(\hat{a}_k = a_k, \hat{i}_k = i_k)$, ii) ULA and IRS are detected incorrectly: $(\hat{a}_k \neq a_k, \hat{i}_k \neq i_k)$, iii) ULA is detected incorrectly but IRS is detected correctly: $(\hat{a}_k \neq a_k, \hat{i}_k = i_k)$, iv) ULA is detected correctly but IRS is detected incorrectly: $(\hat{a}_k = a_k, \hat{i}_k \neq i_k)$.

A. Case 1 $(\hat{a}_k = a_k, \hat{i}_k = i_k)$

In this case, $|y_{\hat{k}} - \sqrt{P_k} \mathbf{w}_{\hat{a}_k,\hat{i}_k,\hat{k}}^H \mathbf{Y}_{\hat{a}_k,\hat{i}_k,\hat{k}} \mathbf{f}_{\hat{a}_k,\hat{i}_k,\hat{k}} \hat{s}_k|^2$ is as follows:

$$\begin{aligned} &\Big| \sqrt{P_k} \mathbf{w}_{a_k,i_k,k}^H \mathbf{Y}_{a_k,i_k,k} \mathbf{f}_{a_k,i_k,k} s_k + \mathbf{w}_{a_k,i_k,k}^H \mathbf{n}_k \\ &- \sqrt{P_k} \mathbf{w}_{a_k,i_k,k}^H \mathbf{Y}_{a_k,i_k,k} \mathbf{f}_{a_k,i_k,k} \hat{s}_k \Big|^2 \\ &= \left| \mathbf{w}_{a_k,i_k,k}^H \mathbf{n}_k + \sqrt{P_k} \mathbf{w}_{a_k,i_k,k}^H \mathbf{Y}_{a_k,i_k,k} \mathbf{f}_{a_k,i_k,k} (s_k - \hat{s}_k) \right|^2. \end{aligned} \tag{19}$$

The average PEP expression is calculated as $P(\{a_k, i_k, s_k\} \rightarrow \{a_k, i_k, \hat{s}_k\} | \{a_k, i_k, s_k\}) = P(\gamma < 0)$. $\gamma = 2\,\mathrm{Re}\{\mathbf{n}_k^H \mathbf{w}_{a_k,i_k,k}^H \mathbf{w}_{a_k,i_k,k} \mathbf{n}_k \mathbf{Y}_{a_k,i_k,k} \mathbf{f}_{a_k,i_k,k} (s_k - \hat{s}_k)\} + |\mathbf{w}_{a_k,i_k,k}^H \mathbf{Y}_{a_k,i_k,k} \mathbf{f}_{a_k,i_k,k} (s_k - \hat{s}_k)|^2$ with the $\gamma \sim \mathcal{CN}(\mu_\gamma, \sigma_\gamma^2)$ distribution. After calculating the mean and variance values, the final average PEP is obtained as follows:

$$\begin{aligned} &P\left(\{a_k, i_k, s_k\} \rightarrow \{a_k, i_k, \hat{s}_k\} | \{a_k, i_k, s_k\}\right) \\ &= Q\left(\sqrt{\frac{\|\mathbf{Y}_{a_k,i_k,k} f_{a_k,i_k,k} (s_k - \hat{s}_k)\|^2}{2\sigma^2}} \right). \end{aligned} \tag{20}$$

[2]In this study, PEP is employed for error analysis, since the possibility of more than one incorrect detection in the receiver determines whether the transmitted symbol is received correctly or not.

$$\mathbf{Y}_{eff} = \begin{bmatrix} \mathbf{w}_{a_1,i_1,1}^H \mathbf{Y}_{a_1,i_1,1} \mathbf{f}_{a_1,i_1,1} & \cdots & \mathbf{w}_{a_1,i_1,1}^H \mathbf{Y}_{a_C,i_C,1} \mathbf{f}_{a_C,i_C,C} \\ \vdots & \ddots & \vdots \\ \mathbf{w}_{a_C,i_C,C}^H \mathbf{Y}_{a_1,i_1,C} \mathbf{f}_{a_1,i_1,1} & \cdots & \mathbf{w}_{a_C,i_C,C}^H \mathbf{Y}_{a_C,i_C,C} \mathbf{f}_{a_C,i_C,C} \end{bmatrix} \tag{14}$$

B. Case 2 ($\hat{a}_k \neq a_k, \hat{i}_k \neq i_k$)

In this case, $|y_{\hat{k}} - \sqrt{P_{\hat{k}}}\mathbf{w}^H_{\hat{a}_k,\hat{i}_k,\hat{k}}\mathbf{Y}_{\hat{a}_k,\hat{i}_k,\hat{k}}\mathbf{f}_{\hat{a}_k,\hat{i}_k,\hat{k}}\hat{s}_k|^2$ is as follows:

$$\left|\sqrt{P_{\hat{k}}}\mathbf{w}^H_{\hat{a}_k,\hat{i}_k,\hat{k}}\ \mathbf{Y}_{\hat{a}_k,\hat{i}_k,\hat{k}}(\mathbf{f}_{a_k,i_k,k}s_k - \mathbf{f}_{\hat{a}_k,\hat{i}_k,\hat{k}}\hat{s}_k) + \mathbf{w}^H_{\hat{a}_k,\hat{i}_k,\hat{k}}\mathbf{n}_k\right|^2. \tag{21}$$

The average PEP expression is calculated as follows:

$$\begin{aligned} &P\left(\{a_k, i_k, s_k\} \to \left\{\hat{a}_k, \hat{i}_k, \hat{s}_k\right\} |\{a_k, x_k, s_k\}\right) \\ &= P\left(\left|\sqrt{P_k}\mathbf{w}^H_{\hat{a}_k,\hat{i}_k,\hat{k}}\mathbf{Y}_{\hat{a}_k,\hat{i}_k,\hat{k}}\left(\mathbf{f}_{a_k,i_k,k}s_k - \mathbf{f}_{\hat{a}_k,\hat{i}_k,\hat{k}}\hat{s}_k\right)\right.\right. \\ &\quad \left.\left. + \mathbf{w}^H_{\hat{a}_k,\hat{i}_k,\hat{k}}\mathbf{n}_k\right|^2 - \left|\mathbf{w}^H_{a_k,i_k,k}\mathbf{n}_k\right|^2 < 0\right). \end{aligned} \tag{22}$$

Here, let it be defined as $\dot{\beta}_1 = |\sqrt{P_k}\mathbf{w}^H_{\hat{a}_k,\hat{i}_k,\hat{k}}\mathbf{Y}_{\hat{a}_k,\hat{i}_k,\hat{k}}(\mathbf{f}_{a_k,i_k,k}s_k - \mathbf{f}_{\hat{a}_k,\hat{i}_k,\hat{k}}\hat{s}_k)|^2 + |\mathbf{w}^H_{\hat{a}_k,\hat{i}_k,\hat{k}}\mathbf{n}_k|^2$ and $\dot{\beta}_2 = |\mathbf{w}^H_{a_k,i_k,k}\mathbf{n}_k|^2$.

Then, $\dot{Chi}_1 \triangleq \frac{2\dot{\beta}_1}{\sigma^2}$ and $\dot{Chi}_2 \triangleq \frac{2\dot{\beta}_2}{\sigma^2}$ definitions, it is seen that $\dot{Chi}_1$ is a 2-degrees-of-freedom chi-square distribution with a decentralization parameter $\dot{\lambda} = \frac{2|\sqrt{P_k}\mathbf{w}^H_{\hat{a}_k,\hat{i}_k,\hat{k}}\mathbf{Y}_{\hat{a}_k,\hat{i}_k,\hat{k}}(\mathbf{f}_{a_k,i_k,k}s_k - \mathbf{f}_{\hat{a}_k,\hat{i}_k,\hat{k}}\hat{s}_k)|^2}{\sigma^2}$. Similarly, $\dot{Chi}_2$ has a central chi-square distribution with 2 degrees of freedom. Alternatively, it can be written as an exponential distribution with a parameter of $\frac{1}{2}$:

$$\begin{aligned} &P\left(\{a_k, i_k, s_k\} \to \left\{\hat{a}_k, \hat{i}_k, \hat{s}_k\right\} |\{a_k, i_k, s_k\}\right) \\ &= P\left(\dot{Chi}_1 < \dot{Chi}_2\right) = \frac{1}{2}e^{-\frac{\dot{\lambda}}{4}}. \end{aligned} \tag{23}$$

C. Case 3 ($\hat{a}_k = a_k, \hat{i}_k \neq i_k$)

Similar to the analysis in (B), the average PEP expression of this case for $\ddot{\lambda} = \frac{2|\sqrt{P_k}\mathbf{w}^H_{a_k,\hat{i}_k,\hat{k}}\mathbf{Y}_{a_k,\hat{i}_k,\hat{k}}(\mathbf{f}_{a_k,i_k,k}s_k - \mathbf{f}_{a_k,\hat{i}_k,\hat{k}}\hat{s}_k)|^2}{\sigma^2}$ results in:

$$\begin{aligned} &P\left(\{a_k, i_k, s_k\} \to \left\{a_k, \hat{i}_k, \hat{s}_k\right\} |\{a_k, i_k, s_k\}\right) \\ &= P\left(\ddot{Chi}_1 < \ddot{Chi}_2\right) = \frac{1}{2}e^{-\frac{\ddot{\lambda}}{4}}. \end{aligned} \tag{24}$$

D. Case 4 ($\hat{a}_k \neq a_k, \hat{i}_k = i_k$)

Similar to the previous analysis, the average PEP expression of this case for $\tilde{\lambda} = \frac{2|\sqrt{P_k}\mathbf{w}^H_{\hat{a}_k,i_k,\hat{k}}\mathbf{Y}_{\hat{a}_k,i_k,\hat{k}}(\mathbf{f}_{a_k,i_k,k}s_k - \mathbf{f}_{\hat{a}_k,i_k,\hat{k}}\hat{s}_k)|^2}{\sigma^2}$ results in:

$$\begin{aligned} &P\left(\{a_k, i_k, s_k\} \to \{\hat{a}_k, i_k, \hat{s}_k\} |\{a_k, i_k, s_k\}\right) \\ &= P\left(\tilde{Chi}_1 < \tilde{Chi}_2\right) = \frac{1}{2}e^{-\frac{\tilde{\lambda}}{4}}. \end{aligned} \tag{25}$$

Let the general names of the average PEP equations given in (20), (23), (24) and (25) for these four cases be considered Pr_e. In addition, let the number of erroneous bits that occur after these four cases occur be ε_b, the total number of implementations be N and the total number of transmitted bits be b_t. In this case, BER P_{BER} can be limited as:

$$P_{BER} \leq \frac{1}{n_b N} \sum_{\begin{Bmatrix} a_k \\ i_k \\ s_k \end{Bmatrix}} \sum_{\begin{Bmatrix} \hat{a}_k \\ \hat{i}_k \\ \hat{s}_k \end{Bmatrix}} \varepsilon_b Pr_e. \tag{26}$$

As a result, the BER analysis is completed using the average PEP analysis of these four cases.

IV. Achievable Rate Analysis

The mutual information between the transmitted and received symbols is $I(y_k; x_k) = H(y_k) - H(y_k|x_k)$, where x_k represents the information symbol that includes the indices of the IRS, ULA, and symbol. The received signal y_k has a Gaussian mixture distribution and there is no closed-form solution to the entropy of a Gaussian mixture. Therefore, it would be a better choice to employ SNR-based rate analysis instead of information theory-based one. The exact rate of k-th user can be calculated as follows:

$$R_k = \log_2\left(1 + \frac{P_k\left|\mathbf{w}^H_{a_k,i_k,k}\mathbf{Y}_{a_k,i_k,k}\mathbf{f}_{a_k,i_k,k}\right|^2}{\sigma^2}\right), \tag{27}$$

where P_k is the power of k-th user. As a result, the total achievable rate of the system is $R_{tot} = \sum_{k=1}^{C} R_k$ as identical distribution of the fading channels is experienced by the C users.

Lemma: Let $Y = R + jI$ be a complex random variable consisting of two independent Gaussian mixture distributions R and I with the same number N of equiprobable Gaussian distributions each with mean $\Re e[\mu_n]$, $\Im m[\mu_n]$ and identical variance σ^2. The distribution function of Y is

$$f_Y(y) = \frac{1}{\sigma\pi N}\sum_{n=1}^{N} e^{-\frac{|y-\mu_n|^2}{\sigma}^2}, \tag{28}$$

where $\mu_n = \Re e[\mu_n] + j\Im m[\mu_n]$. In this case, the variance of Y is as follows:

$$\begin{aligned} Var(Y) &= 2\sigma^2 + \frac{1}{N}\sum_{n=1}^{N}|\mu_n|^2 - \frac{1}{N^2}\left(\sum_{n=1}^{N}\Re e[\mu_n]\right)^2 \\ &\quad - \frac{1}{N^2}\left(\sum_{n=1}^{N}\Im m[\mu_n]\right)^2. \end{aligned} \tag{29}$$

Proof: See Appendix.

The detection of indices of the IRS and ULA and of the symbol are independent events and the probability density function of the received signal at the k-th user, $f_{Y_k}(y_k)$, can thus be written in accordance to the above Lemma as follows:

$$f_{Y_k}(y_k) = \frac{1}{\sigma\pi X N_U M}\sum_{t=1}^{X}\sum_{z=1}^{N_U}\sum_{m=1}^{M} e^{-\frac{|y_k-\mu_{y_k}|^2}{\sigma^2_{Y_k}}}, \tag{30}$$

where $\mu_{y_k} = \sqrt{P_k}\mathbf{w}^H_{z,t,k}\mathbf{Y}_{z,t,k}\mathbf{f}_{z,t,k}s_m$.

We know that the differential entropy of any random variable with finite variance is less than or equal to the differential entropy

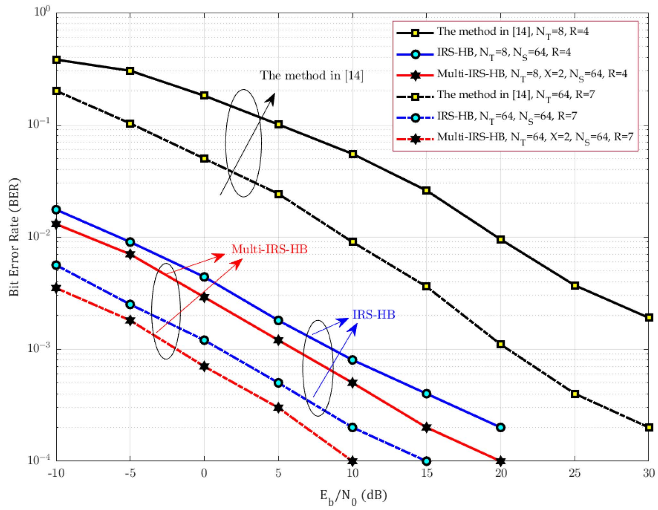

Fig. 2. BER performances comparison of Multi-IRS-HB, IRS-HB and the method in [14] for $C = 2, N_R = 1, N_U = 4$, and $4 - QAM$.

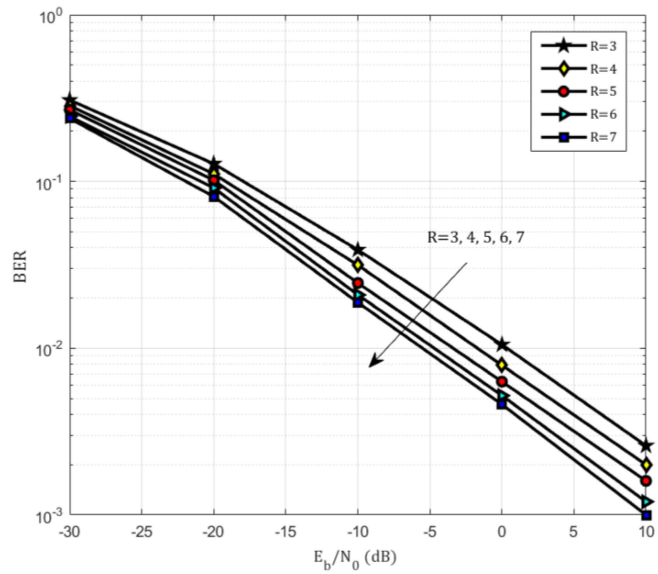

Fig. 3. BER performances comparison of Multi-IRS-HB, IRS-HB and the method in [14] for $C = 2, N_R = 1, N_T = 8, N_U = 4, X = 2, N_S = 32$, and $4 - QAM$.

of a Gaussian random variable with the same variance [29]. It is then possible to obtain an upper bound for the achievable rate.

Theorem: The achievable rate R_k of the k-th user receiving s_m symbols transmitted by the base station selected from M-ary spatially modulated discrete input symbols is upper bounded by R'_k:

$$\begin{aligned} R'_k = \log_2 \Bigg(\pi e \Bigg(& 2\sigma^2 + \frac{P_k}{X N_U M} \sum_{t=1}^{X} \sum_{z=1}^{N_U} \sum_{m=1}^{M} |\Lambda_{z,t,k,m}|^2 \\ & - \frac{P_k}{X^2 N_U^2 M^2} \left[\sum_{t=1}^{X} \sum_{z=1}^{N_U} \sum_{m=1}^{M} \Re e \left\{ \Lambda_{z,t,k,m} \right\} \right]^2 \\ & - \frac{P_k}{X^2 N_U^2 M^2} \left[\sum_{t=1}^{X} \sum_{z=1}^{N_U} \sum_{m=1}^{M} \Im m \left\{ \Lambda_{z,t,k,m} \right\} \right]^2 \Bigg) \Bigg) \\ & - \log_2 \left(\pi e \sigma^2 \right), \end{aligned} \tag{31}$$

where $\Lambda_{z,t,k,m} = \mathbf{w}_{z,t,k}^H \mathbf{Y}_{z,t,k} \mathbf{f}_{z,t,k} s_m$ and $k \in \{1, 2, \ldots, C\}$.

Proof: See Appendix.

V. Simulation Results

This section evaluates the performance of the proposed system through computer simulations. The simulation results are presented in two subsections, such as classical channel model and real physical channel model. The path loss in the real physical channel model is considered according to the 5G UMi-Street Canyon and 5G InH Indoor-Office models, while the path loss of the RF carrier is ignored in the classical channel model. In all simulations, we assume that $C = 2$, $N_R = 1$ and that the symbols are *4-QAM* modulated.

A. Simulation Results for Classical Channel Model

For all simulations in this subsection, we assume that $L_D = 3$, $L_G = 3$, and $L_H = 1$. In Fig. 2, the BER performances of Multi-IRS-HB, IRS-HB (single IRS) and the method in [14] are compared for $N_T = 8$ and $N_T = 64$ transmit antennas. According to this figure, Multi-IRS-HB performs much better than IRS-HB model and the spatial modulated hybrid beamforming scheme in [14]. As can be seen from this figure, the BER performance improves significantly as the number of transmit antennas increases, because the beam can then be directed better. When $N_S = 64$, Multi-IRS-HB gains about 22–25 dB compared to the method in [14] for $N_T = 64$ and $N_T = 8$ respectively.

The impact of the resolution of the phase shifters on the performance of the Multi-IRS-HB system is demonstrated in Fig. 3. The figure illustrates that the BER performance improves as the bit resolution R increases. As resolution increases, the quantization error decreases, resulting in improved error performance. Selecting the highest value is not feasible due to cost and practical limitations.[3]

Fig. 4 shows the impact of different active IRS selections on the BER performance of the proposed system. The performance curves are quite close, indicating that the active IRS during communication does not significantly impact the system performance.

Fig. 5 presents the simulation results analyzing whether Multi-IRS-HB and the model in [14] attain their respective theoretical BER curves. The figure shows that the BER curve of Multi-IRS-HB closely approximates to its theoretical curve.

Fig. 6 displays the achievable rate performance of Multi-IRS-HB, which outperforms the method presented in [14] with higher SE. The data rate is expressed in bits per channel utilization (bpcu) as $\eta = \log_2(M) + \log_2(N_U) + \log_2(X)$. It is evident that an increase in the number of IRSs and ULAs will have a positive effect on the achievable rate.

[3]The best bit resolutions can be empirically determined, for Multi-IRS-HB, such as $R = 4$ for $N_T = 8$ and $R = 7$ for $N_T = 64$.

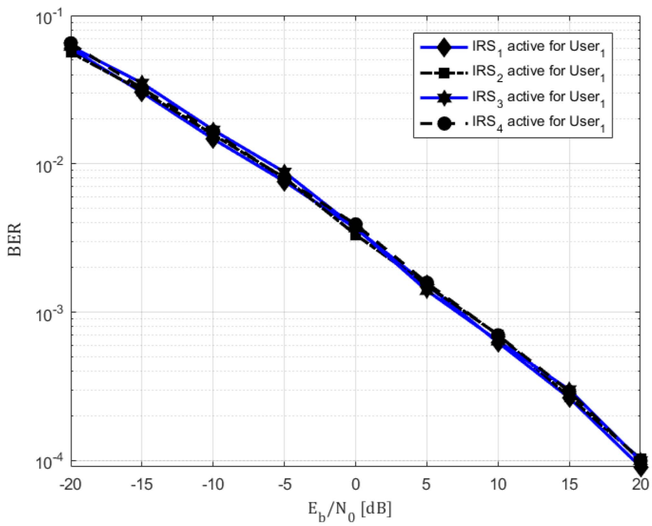

Fig. 4. BER performances of the proposed system with different IRS selections for $C = 2, N_R = 1, N_T = 8, N_U = 4, X = 4, N_S = 32, R = 5,$ and $4 - QAM$.

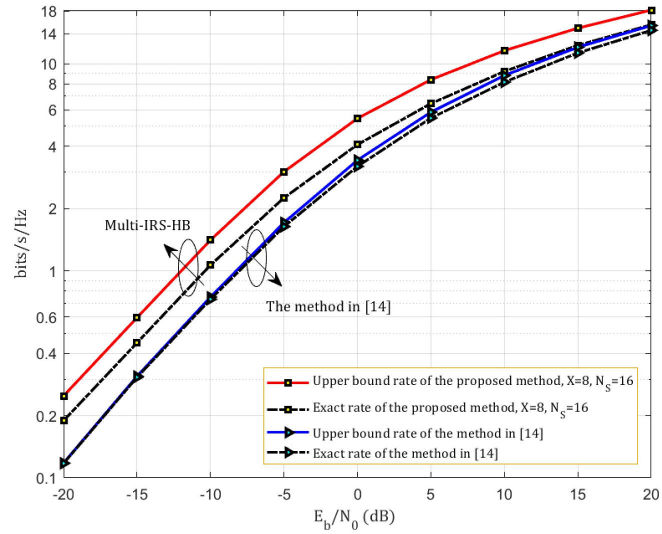

Fig. 6. Total achievable rate performances of Multi-IRS-HB and the method in [14] for $C = 2, N_R = 1, N_T = 8, N_U = 2, R = 4,$ and $4 - QAM$.

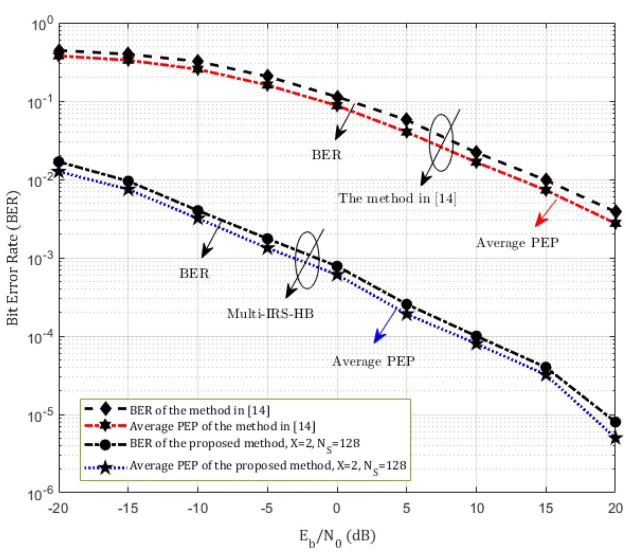

Fig. 5. BER performances of Multi-IRS-HB and the method in [14] for $C = 2, N_R = 1, N_T = 16, N_U = 4, R = 6,$ and $4 - QAM$.

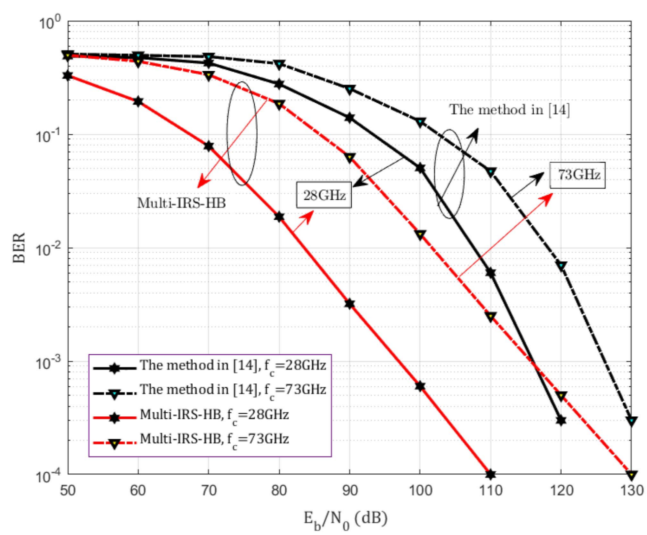

Fig. 7. BER performances comparison of Multi-IRS-HB and the method in [14] under indoor path loss at $f_c = 28\,\text{GHz}$ and $f_c = 73\,\text{GHz}$.

B. Simulation Results for Real Physical Channel Model

In this subsection, we assume $L_D = 2$, $L_G = 2$, $L_H = 2$ for all simulations. The antenna gain of the IRS in both the transmit and receive directions is defined as 3 dBi for indoor and 5 dBi for outdoor environments, as stated in references [23], [28].

Fig. 7 shows a comparison of the BER performance between Multi-IRS-HB and the method described in [14] at $f_c = 28\,\text{GHz}$ and $f_c = 73\,\text{GHz}$ using the 5G InH Indoor-Office path loss model (9), (10) for the indoor scenario. The system parameters are defined as $C = 2$, $N_R = 1$, $N_T = 4$, $N_U = 2$, $X = 2$, $N_S = 512$ and $R = 4$. The method in [14] only considers the L_D path, while the proposed system model considers three path links: L_D, L_G, and L_H. Distances are generated separately for each user in the system. The first user is referred to as C_1 and the second user as C_2. The first MS is referred to as MS_1 and the second MS as MS_2. The distances in meters are determined as follows:

- For L_D, the distances of the links BS-MS_1 and BS-MS_2 can be represented in vector form as $\mathbf{l}_{d_{Gi_1}} = [4\ \ 5]$ and $\mathbf{l}_{d_{Gi_2}} = [6\ \ 8]$, respectively. The columns of the vector display the first and second distances l_{d_1} and l_{d_2}, representing line-of-sight (LOS) and non-line-of-sight (NLOS) distances, respectively.
- For L_G, the distance vector of the BS-IRS_1 link is determined as $\mathbf{l}_{g_{C_1}} = [1.5\ \ 2]$ for the C_1 and the distance vector of the BS-IRS_2 link is determined as $\mathbf{l}_{g_{C_2}} = [2.5\ \ 3]$ for the C_2. The distance vectors of the IRS-MS_1 and IRS-MS_2 links for L_H are $\mathbf{l}_{h_{Gi_1}} = [2\ \ 2.5]$ and $\mathbf{l}_{h_{Gi_2}} = [3\ \ 3.5]$, respectively.

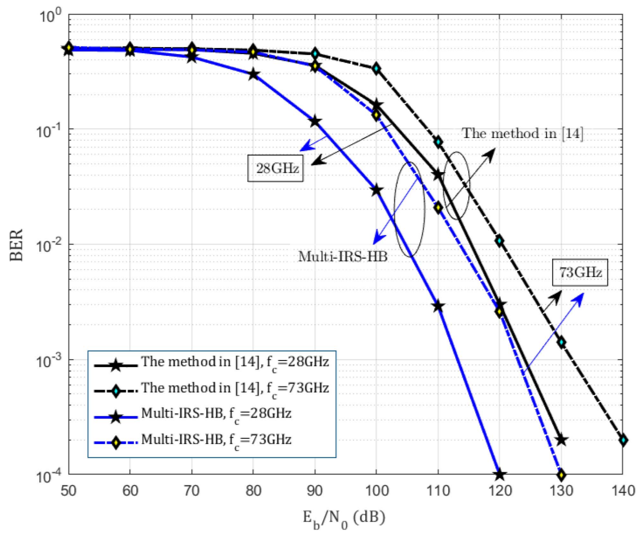

Fig. 8. BER performances comparison of Multi-IRS-HB and the method in [14] under outdoor path loss at $f_c = 28\,\text{GHz}$ and $f_c = 73\,\text{GHz}$.

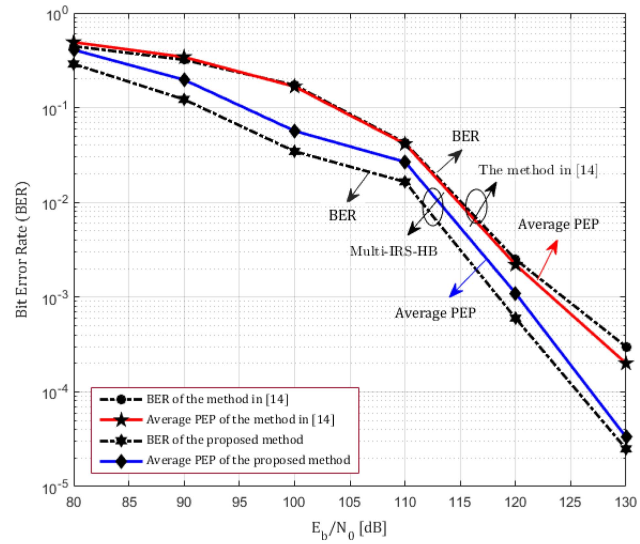

Fig. 9. BER performances of Multi-IRS-HB and the method in [14] under path loss at $f_c = 28\,\text{GHz}$.

As can be seen from the figure, the proposed system performs better compared to the method in [14], providing a gain of approximately 25 dB at 28 GHz and approximately 18 dB at 73 GHz. Fig. 8 also shows a comparison of the BER performance between Multi-IRS-HB and the method described in [14] at $f_c = 28\,\text{GHz}$ and $f_c = 73\,\text{GHz}$ using the 5G UMi-Street Canyon path loss model (11), (12) for an outdoor scenario. The system parameters are defined as $C = 2$, $N_R = 1$, $N_T = 32$, $N_U = 2$, $X = 2$, $N_S = 1024$ and $R = 6$. The distances in meters are determined as follows:

- For L_D, the distance of the links BS-MS$_1$ and BS-MS$_2$ can be represented in vector form as $\mathbf{l}_{d_{Gi_1}} = [23\ \ 25]$ and $\mathbf{l}_{d_{Gi_2}} = [27\ \ 29]$, respectively.
- For L_G, the distance vector of the BS-IRS link for both users is determined as $\mathbf{l}_g = [10\ \ 11]$. The distance vectors of the IRS-MS$_1$ and IRS-MS$_2$ links for L_H are $\mathbf{l}_{h_{Gi_1}} = [13\ \ 14]$ and $\mathbf{l}_{h_{Gi_2}} = [15\ \ 16]$.

As can be seen from the figure, the proposed system performs better than the method in [14], providing about 11 dB at 28 GHz and 7 dB at 73 GHz, respectively. Figs. 7 and 8 also show how the BER performance of the system operating at different frequencies changes in both indoor and outdoor scenarios for signals transmitted over a real physical channel. It can be seen that the performance deteriorates with increasing frequency from 28 GHz to 73 GHz in both indoor and outdoor scenario simulations. This can be easily seen from (9), (10), (11) and (12), where the path losses in these equations also increase with increasing frequency. These path losses cause the gains of the channels given in (6), (7) and (8) to decrease significantly. As a result, the system performance degrades with increasing frequency.

Fig. 9 shows how closely the BER and theoretical BER curves at 28 GHz for our proposed system model and the model in [14] converge under the 5G UMi-Street Canyon path loss model. The system parameters and distance values used in this simulation are the same as those used in Fig. 8. As can be seen from the figure, the simulated BER curve of the proposed system converges to its theoretical one and shows better error performance compared to the method in [14].

VI. Conclusion

We have proposed an Ls-MIMO communication system that utilizes IRSs to improve the downlink communication performance in the mmWave band. By including SM to the system model, the IRSs' and ULAs' indices are transmitted in the signal, thus increasing the SE. Theoretical analysis of the proposed model is presented, including expressions for theoretical BER and achievable rate, as well as the design of the precoder, beamformer, and combiner. An upper bound for the achievable rate is also derived. The system performance of the proposed system model in the path loss scenario was also examined to experience a real physical radio channel both outdoors and indoors. Simulation results demonstrate that the proposed model achieves close to theoretical limits in terms of performance metrics, and outperforms a similar model based on index modulation [14]. Overall, the results suggest that incorporating IRS into mmWave Ls-MIMO systems which is our proposed Multi-IRS-HB model, can significantly improve communication performance.

Appendix

A. *Proof of Lemma*

The mean and the second moment of Y with respect to the origin can be calculated respectively as follows:

$$E[Y] = \int_{-\infty}^{\infty} y f_Y(y)dy = \frac{1}{N}\sum_{n=1}^{N}\int_{-\infty}^{\infty} y f_{Y_y}(y)$$

$$= \frac{1}{N}\sum_{n=1}^{N}\left(\Re e[\mu_n]\ + j\Im m[\mu_n]\right). \tag{A.1}$$

and

$$E[Y^2] = \frac{1}{N}\sum_{n=1}^{N}\int_{-\infty}^{\infty} y^2 f_{Y_n}(y)$$
$$= \frac{1}{N}\sum_{n=1}^{N}\left(|\mu_n|^2 + 2\sigma^2\right) = 2\sigma^2 + \frac{1}{N}\sum_{n=1}^{N}|\mu_n|^2. \quad \text{(A.2)}$$

Using these last two expressions with $Var(Y) = E[Y^2] - E[Y]E[Y]^*$, the variance of Y can be easily found:

$$Var(Y) = 2\sigma^2 + \frac{1}{N}\sum_{n=1}^{N}|\mu_n|^2 - \frac{1}{N^2}\left(\sum_{n=1}^{N}\Re e[\mu_n]\right)^2 - \frac{1}{N^2}\left(\sum_{n=1}^{N}\Im m[\mu_n]\right)^2. \quad \text{(A.3)}$$

B. Proof of Theorem

The probability density function of the signal received at the k-th user in (16) can be written as follows:

$$f_{Y_k}(y_k) = \frac{1}{XN_UM} f_{Y_k}(i_x = t, a_v = z, s = s_m) \times \sum_{t=1}^{X}\sum_{z=1}^{N_U}\sum_{m=1}^{M} Pr(i_x = t, a_v = z, s = s_m). \quad \text{(A.4)}$$

Since the selection of the IRS index, the selection of the antenna array index, and the M-ary symbols are independent events, the combined probability density function in the above expression can be written as the product of the individual probability density functions:

$$\frac{1}{XN_UM}\sum_{t=1}^{X}\sum_{z=1}^{N_U}\sum_{m=1}^{M} Pr(a_x = t, a_v = z, s = s_m)$$
$$= \frac{1}{XN_UM} \times \sum_{t=1}^{X}\sum_{z=1}^{N_U}\sum_{m=1}^{M} Pr(a_x = t)Pr(a_v = z), Pr(s = s_m). \quad \text{(A.5)}$$

Since the selection probabilities of any IRS, any antenna array and any symbol from the M-alphabet are equal, these selections can be expressed by the uniform distributions $U(1, X)$, $U(1, N_U)$, $U(1, M)$. Then, the probability density function of Y_k can be written as:

$$f_{Y_k}(y_k) = \frac{1}{\sigma\pi XN_UM} \times \sum_{t=1}^{X}\sum_{z=1}^{N_U}\sum_{m=1}^{M} e^{-\frac{\left|y_k - \sqrt{P_k} w_{z,t,k}^H Y_{z,t,k} f_{z,t,k} s_m\right|^2}{\sigma_{Y_k}^2}}. \quad \text{(A.6)}$$

It is the probability density function of a Gaussian mixture distribution with mean $\sqrt{P_k}\mathbf{w}_{z,t,k}^H\mathbf{Y}_{z,t,k}\mathbf{f}_{z,t,k}s_m$ and variance $\sigma_{Y_k}^2$. Using the lemma, the variance of the distribution can be easily written as:

$$\sigma_{Y_k}^2 = 2\sigma^2 + \frac{P_k}{XN_UM}\sum_{t=1}^{X}\sum_{z=1}^{N_U}\sum_{m=1}^{M}\left|\mathbf{w}_{z,t,k}^H\mathbf{Y}_{z,t,k}\mathbf{f}_{z,t,k}s_m\right|^2 - \frac{P_k}{X^2N_U^2M^2}\left[\sum_{t=1}^{X}\sum_{z=1}^{N_U}\sum_{m=1}^{M}\mathrm{Re}\left\{\left|\mathbf{w}_{z,t,k}^H\mathbf{Y}_{z,t,k}\mathbf{f}_{z,t,k}s_m\right|\right\}\right]^2 - \frac{P_k}{X^2N_U^2M^2}\left[\sum_{t=1}^{X}\sum_{z=1}^{N_U}\sum_{m=1}^{M}\mathrm{Im}\left\{\left|\mathbf{w}_{z,t,k}^H\mathbf{Y}_{z,t,k}\mathbf{f}_{z,t,k}s_m\right|\right\}\right]^2. \quad \text{(A.7)}$$

Keeping in mind the fact that the differential entropy of any random variable with finite variance is less than or equal to the differential entropy of a Gaussian random variable with the same variance [29], the achievable rate R_k has upper bounded by:

$$R_k \le R_k' = \log_2\Bigg(\pi e\Bigg(2\sigma^2 + \frac{P_k}{XN_UM}\sum_{t=1}^{X}\sum_{z=1}^{N_U}\sum_{m=1}^{M}|\Lambda_{z,t,k,m}|^2 - \frac{P_k}{X^2N_U^2M^2}\left[\sum_{t=1}^{X}\sum_{z=1}^{N_U}\sum_{m=1}^{M}\Re e\left\{\Lambda_{z,t,k,m}\right\}\right]^2 - \frac{P_k}{X^2N_U^2M^2}\left[\sum_{t=1}^{X}\sum_{z=1}^{N_U}\sum_{m=1}^{M}\Im m\left\{\Lambda_{z,t,k,m}\right\}\right]^2\Bigg)\Bigg) - \log_2\left(\pi e\sigma^2\right), \quad \text{(A.8)}$$

where $\Lambda_{z,t,k,m} = \mathbf{w}_{z,t,k}^H\mathbf{Y}_{z,t,k}\mathbf{f}_{z,t,k}s_m$ and $k \in \{1, 2, \ldots, C\}$.

References

[1] W. Hong et al., "The role of millimeter-wave technologies in 5G/6G wireless communications," *IEEE J. Microw.*, vol. 1, no. 1, pp. 101–122, Jan. 2021.

[2] S. A. Busari, K. M. S. Huq, S. Mumtaz, L. Dai, and J. Rodriguez, "Millimeter-wave massive MIMO communication for future wireless systems: A survey," *IEEE Commun. Surveys Tuts.*, vol. 20, no. 2, pp. 836–869, Secondquarter 2018.

[3] I. Ahmed et al., "A survey on hybrid beamforming techniques in 5G: Architecture and system model perspectives," *IEEE Commun. Surveys Tuts.*, vol. 20, no. 4, pp. 3060–3097, Fourthquarter 2018.

[4] R. Dilli, "Hybrid beamforming in 5G NR networks using multi user massive MIMO at FR2 frequency bands," *Wireless Pers. Commun.*, vol. 127, no. 4, pp. 3677–3709, 2022.

[5] S. Gong et al., "Hardware-impaired RIS-assisted mmWave hybrid systems: Beamforming design and performance analysis," *IEEE Trans. Commun.*, vol. 71, no. 4, pp. 2317–2334, Apr. 2023.

[6] Q. Zhu, H. Li, R. Liu, M. Li, and Q. Liu, "Hybrid beamforming and passive reflection design for RIS-assisted mmWave MIMO systems," in *Proc. IEEE Int. Conf. Commun. Workshops*, 2021, pp. 1–6.

[7] S. H. Hong, J. Park, S.-J. Kim, and J. Choi, "Hybrid beamforming for intelligent reflecting surface aided millimeter wave MIMO systems," *IEEE Trans. Wireless Commun.*, vol. 21, no. 9, pp. 7343–7357, Sep. 2022.

[8] R. Dilli, "Performance analysis of multi user massive MIMO hybrid beamforming systems at millimeter wave frequency bands," *Wireless Netw.*, vol. 27, no. 3, pp. 1925–1939, 2021.

[9] Z. Li, T. Chen, and X. Hu, "Hybrid beamforming for millimeter-wave massive MIMO heterogeneous networks," *Digit. Signal Process.*, vol. 130, 2022, Art. no. 103738.

[10] N. K. Daghari, T. Y. Elganimi, and K. M. Rabie, "Energy-efficient hybrid precoding schemes for RIS-assisted millimeter-wave massive MIMO," in *Proc. IEEE Int. Mediterranean Conf. Commun. Netw.*, 2021, pp. 294–299.
[11] J. C. Chen, "Hybrid beamforming with discrete phase shifters for millimeter-wave massive MIMO systems," *IEEE Trans. Veh. Technol.*, vol. 66, no. 8, pp. 7604–7608, Aug. 2017.
[12] S. Thurpati and P. Muthuchidambaranathan, "Design of hybrid precoder for mm-Wave MIMO system based on generalized triangular decomposition method," *Int. J. Electron. Telecommun.*, vol. 68, no. 3, pp. 519–525, 2022.
[13] A. M. Elbir, S. Coleri, and K. V. Mishra, "Federated dropout learning for hybrid beamforming with spatial path index modulation in multi-user mmWave-MIMO systems," in *Proc. IEEE Int. Conf. Acoust., Speech Signal Process.*, 2021, pp. 8213–8217.
[14] M. Yüzgeccioğlu and E. Jorswieck, "Hybrid beamforming with spatial modulation in multi-user massive MIMO mmWave networks," in *Proc. IEEE 28th Annu. Int. Symp. Pers., Indoor, Mobile Radio Commun.*, 2017, pp. 1–6.
[15] W. Yan, X. Yuan, Z. -Q. He, and X. Kuai, "Passive beamforming and information transfer design for reconfigurable intelligent surfaces aided multiuser MIMO systems," *IEEE J. Sel. Areas Commun.*, vol. 38, no. 8, pp. 1793–1808, Aug. 2020.
[16] T. Zhou et al., "Aerial intelligent reflecting surface-enhanced cell-free massive MIMO for high-mobility communication: Joint Doppler compensation and power optimization," *EURASIP J. Adv. Signal Process.*, vol. 2021, pp. 1–18, 2021.
[17] Z. Yang, W. Xu, C. Huang, J. Shi, and M. Shikh-Bahaei, "Beamforming design for multiuser transmission through reconfigurable intelligent surface," *IEEE Trans. Wireless Commun.*, vol. 69, no. 1, pp. 589–601, Jan. 2021.
[18] S. Gong, C. Xing, P. Yue, L. Zhao, and T. Q. S. Quek, "Hybrid analog and digital beamforming for RIS-assisted mmWave communications," *IEEE Trans. Wireless Commun.*, vol. 22, no. 3, pp. 1537–1554, Mar. 2023.
[19] S. Abeywickrama, R. Zhang, Q. Wu, and C. Yuen, "Intelligent reflecting surface: Practical phase shift model and beamforming optimization," *IEEE Trans. Commun.*, vol. 68, no. 9, pp. 5849–5863, Sep. 2020.
[20] C. Feng, W. Shen, J. An, and L. Hanzo, "Joint hybrid and passive RIS-assisted beamforming for mmWave MIMO systems relying on dynamically configured subarrays," *IEEE Internet Things J.*, vol. 9, no. 15, pp. 13913–13926, Aug. 2022.
[21] R. Li, B. Guo, M. Tao, Y.-F. Liu, and W. Yu, "Joint design of hybrid beamforming and reflection coefficients in RIS-aided mmWave MIMO systems," *IEEE Trans. Commun.*, vol. 70, no. 4, pp. 2404–2416, Apr. 2022.
[22] J. He, K. Yu, Y. Shi, Y. Zhou, W. Chen, and K. B. Letaief, "Reconfigurable intelligent surface assisted massive MIMO with antenna selection," *IEEE Trans. Wireless Commun.*, vol. 21, no. 7, pp. 4769–4783, Jul. 2022.
[23] I. Yildirim, A. Koc, E. Basar, and T. Le-Ngoc, "RIS-aided angular-based hybrid beamforming design in mmWave massive MIMO systems," in *Proc. IEEE Glob. Commun. Conf.*, 2022, pp. 5267–5272.
[24] R. Pal and K. P. Sarawadekar, "Distributed RIS-assisted mmWave multiuser MIMO beamspace system," *AEU-Int. J. Electron. Commun.*, vol. 161, 2023, Art. no. 154560.
[25] J. Wang, Y. -C. Liang, Y. Pei, and X. S. Shen, "Reconfigurable intelligent surface for small cell network," in *Proc. IEEE Glob. Commun. Conf.*, 2021, pp. 1–6.
[26] Q. Zhang, S. Jin, M. McKay, D. Morales-Jimenez, and H. Zhu, "Power allocation schemes for multicell massive MIMO systems," *IEEE Trans. Wireless Commun.*, vol. 14, no. 11, pp. 5941–5955, Nov. 2015.
[27] T. S. Rappaport, Y. Xing, G. R. MacCartney, A. F. Molisch, E. Mellios, and J. Zhang, "Overview of millimeter wave communications for fifth-generation (5G) wireless networks-with a focus on propagation models," *IEEE Trans. Antennas Propag.*, vol. 65, no. 12, pp. 6213–6230, Dec. 2017.
[28] S. W. Ellingson, "Path loss in reconfigurable intelligent surface-enabled channels," in *Proc. IEEE 32nd Annu. Int. Symp. Pers., Indoor Mobile Radio Commun.*, 2021, pp. 829–835.
[29] T. M. Cover and J. A. Thomas, *Elements of Information Theory*. Hoboken, NJ, USA: Wiley, 2006.

Beyza Onal received the B.S. (Highest Hons.) and M.S. degrees in electrical and electronics engineering in 2020 and 2023, respectively, from Istanbul Medeniyet University, Istanbul, Türkiye, where she is currently working toward the Ph.D. degree in electrical and electronics engineering. She is a Research Assistant with the Department of Electrical and Electronics Engineering, Istanbul Medeniyet University. Her main research interests include wireless communications, millimeter-wave, massive MIMO, hybrid beamforming, spatial modulation, index modulation techniques, and intelligent reconfigurable surface (IRS).

Nihat Kabaoglu (Member, IEEE) received the Ph.D. degree in electronics and telecommunication engineering from Istanbul Technical University, Istanbul, Türkiye, in 2005. He is currently a University Professor with the Department of Electrical and Electronics Engineering, Istanbul Medeniyet University, Istanbul. His research interests include statistical signal processing, array processing, wireless networking and communications, application of artificial intelligence and machine learning techniques to wireless communications and networks. His current research interests include channel estimation and data detection, network resource optimization, cognitive radio networks, physical layer security and RF/FSO hybrid systems, intelligent reconfigurable surface (IRS), beamforming design for 5G and next generation systems.